

NUMERICAL MODELS OF MASONRY BASED ON EXPERIMENTAL DATA

Leszek SZOJDA ^a, Grzegorz WANDZIK ^b

^a Faculty of Civil Engineering, The Silesian University of Technology, Akademicka 4, 44-100 Gliwice, Poland
E-mail address: Leszek.Szojda@polsl.pl

^b Faculty of Civil Engineering, The Silesian University of Technology, Akademicka 4, 44-100 Gliwice, Poland
E-mail address: Grzegorz.Wandzik@polsl.pl

Received: 20.11.2007; Revised: 12.12.2007; Accepted: 14.01.2008

Abstract

The authors' intention was to define the failure surface for the masonry for its further use in computational system for nonlinear finite element method analysis. Results of triaxial and uniaxial experimental tests for brick and mortar have been presented in the paper. These results were used as a basis for determination of the failure surfaces in stress space for both materials. Simultaneously, results of laboratory experiments carried out on standard masonry specimens under compression have been presented. These tests were supplemented with computational simulation performed with the use of nonlinear FEM analysis system Mafem3D. Masonry specimen was numerically analysed with use of individual mathematical description of brick and mortar behaviour (heterogeneous model). Calculation of the same specimen with the use of homogeneous material model have been carried out. Shape of the failure surface for homogeneous model was derived from the experimental test results for components (brick and mortar) and masonry specimens. Verification of simulation (made with the use of heterogeneous and homogeneous models as well) results with experimental data was done. Homogeneous material model was formulated because of the necessity of its use in nonlinear FEM analysis of real-scale masonry structures, where size of finite elements exceeds the size of singular masonry units (bricks and joints).

Streszczenie

Zamierzeniem autorów było zdefiniowanie powierzchni granicznej dla muru w celu zastosowania jej w systemie komputerowym do nieliniowych analiz metodą elementów skończonych. W artykule przedstawiono wyniki trójosiowych i jednoosiowych badań cegły i zaprawy. Stanowiły one podstawę do wyznaczenia położenia powierzchni granicznych tych materiałów w przestrzeni naprężeń. Zaprezentowano również rezultaty badań laboratoryjnych standardowych murków poddanych ścisłaniu. Zostały one uzupełnione symulacją komputerową z wykorzystaniem systemu Mafem3d przeznaczonego do nieliniowej analizy MES. Analizie numerycznej poddano mur, w którym cechy poszczególnych materiałów były modelowane niezależnie (model heterogeniczny). Wykonano również obliczenia takiej samej próbki muru z użyciem homogenicznego modelu materiałowego. Kształt powierzchni granicznej homogenicznego modelu materiałowego muru określony został na podstawie wyników badań eksperymentalnych materiałów składowych oraz wyników uzyskanych dla próbek muru. Przeprowadzono weryfikację zgodności wyników obliczeń dla modeli heterogenicznego i homogenicznego z wynikami doświadczalnymi. Stworzenie homogenicznego modelu materiałowego muru wynikało z potrzeby jego zastosowania w nieliniowej analizie większych obiektów wykonanych z cegły, gdzie występuje konieczność tworzenia elementów skończonych o wymiarach większych od wymiarów cegieł i spoin.

Keywords: Masonry; Failure surface; Material model; FEM analysis; Complex stress state.

1. INTRODUCTION

Numerical analysis is accepted way of finding stresses and strains in members of building structures. Obtaining results possibly approximated to the reality requires mathematical description of the material behaviour. It should cover possibly wide range of

complex stress and strain states. Each material model, before its use in analysis of more complicated building structures requires verification on simple models tested in laboratory conditions.

The first step of investigation procedure in numerical analyses is description of appropriate failure surface. A brick and mortar are typical materials which are

used for wall structure. The behaviour of these materials are similar to concrete so the failure surface and characteristic elastic-plastic material description of concrete were adopted to brick and mortar. The detailed description of model used for concrete was published by *Majewski* in [1]. Adoption of concrete failure surface for brick and mortar could be allowed thanks to specific laboratory tests in multiaxial state of stress. Even in typical building structures complex stress state may occur. In such case, description of material properties with the use of only one strength parameter (usually with the use of uniaxial compression strength) is not sufficient. Additional laboratory tests are necessary to obtain parameters describing material behaviour in complex stress state. The tests for description of failure surface separately for brick and mortar were carried out in classical triaxial compression apparatus. Similar tests were conducted by *Drobiec* [2], *Jasiński* [3] and *Piekarczyk* [4]. The phenomena of failure and numerical simulation of brick masonry were recently described in [5], [6] and [7].

Appropriate description of failure surface enables numerical simulation of wall specimens. Because of relatively small size of bricks and joints, individual modelling of these materials in numerical analysis is not possible, especially in case of natural size masonry structures. To enable analysis of masonry, creation of material model substituting individual description of brick and mortar is needed. It is called homogeneous masonry material model. Such a material model, described in this paper was built as a result of actions taken in a few steps. Complete procedure of material model creation was composed of the following steps: laboratory tests of brick and mortar made in triaxial stress state (made individually for each material), tests of masonry samples (carried out according to the rules of standard [8]) subjected to compression. Experimental tests were followed by the numerical analysis of samples used in laboratory tests. Both, heterogeneous (independent individual description for brick and mortar) and homogeneous material models were applied. In model where heterogeneous material model was used, parameters describing bricks and mortar were assumed on the basis of the triaxial laboratory test results. Parameters for the homogeneous description of masonry were assumed in such a way to achieve possibly close agreement for both numerical calculations. Mathematical homogeneous description obtained in the way mentioned above were implemented to computer FEM system called MAFEM3D. In next stage (not presented in this paper), MAFEM3D was applied

to analysis of the small residential building subjected to actions specific for ground subsidence caused by mining excavation [9].

2. Laboratory tests and adopted material model

The tests for brick and mortar were conducted in classical triaxial compression apparatus. Because of peculiarity of this apparatus the shape of specimens had to be a cylinder with diameter 60 mm and height 120 mm. The high compression level demands high accuracy of specimens preparation ($\pm 0,75\text{mm}$). The specimens were closed inside non transparent apparatus and its visual inspection during the tests was impossible. That was the reason why the tests were carried out only in monotonic way – to the failure of specimens. During experiments, the side surface of cylindrical specimen was loaded by increasing pressure of liquid (oil), while bases of cylinder were loaded by pressure of steel plate of testing machine. Vertical and horizontal (longitudinal and circumferential) displacement were recorded during each test. It was enabled by electro-resistance strain gauges which were glued directly on the side surface of the specimens. The irrespective loads in vertical and circumferential directions gave a possibility to perform tests for two types of load paths. In the first loading path, specimen failure was achieved due to increasing of vertical stress (σ_{ver}), while horizontal compression ($\sigma_{hor} = \text{const}$) remained constant. In case of the second loading path, the vertical load had constant value ($\sigma_{ver} = \text{const}$) and specimen failure was caused by increasing of horizontal pressure (σ_{hor}). The relationships in the three-dimensional state of stress can be presented by:

$$\sigma_{hor} = \sigma_1 = \sigma_2 \quad \sigma_{ver} = \sigma_3 \quad (1)$$

The analyzes of tests results are the most efficient when the respective relations are considered in the space of principal stresses. The failure surface in this space is described by mean of normal octahedral stress (σ_{oct}), shear octahedral stress (τ_{ver}) and Lode angle (θ). The relation between horizontal (σ_{hor}) and vertical (σ_{ver}) stresses and octahedral stresses can be presented in the form:

$$\sigma_{oct} = \frac{2\sigma_{hor} + \sigma_{ver}}{3} \quad (2)$$

$$\tau_{oct} = \frac{\sqrt{2}}{3} |\sigma_{hor} - \sigma_{ver}| \quad (3)$$

$$\cos 3\Theta = -SIGN(\sigma_{hor} - \sigma_{ver}) \quad (4)$$

Deviatoric cross-section of a failure surface has threefold rotational symmetry shape. It is repeatable every 120 degrees. The loading paths of experimental tests are entirely contained in two symmetry planes of the surface cross-section. It is caused by the specific relations between principal stresses (1) applied in the experiments. It means that during the tests, there are only two possible Lode angles:

$$\Theta = 0^\circ + \frac{2\pi}{3} \text{ for } \sigma_{hor} < \sigma_{ver} \quad (5)$$

$$\Theta = \frac{\pi}{3} + \frac{2\pi}{3} \text{ for } \sigma_{hor} > \sigma_{ver} \quad (6)$$

The formulas (5) and (6) describe locations of main meridians in the octahedral stress space – compres-

sive meridian for $\sigma_{hor} > \sigma_{ver}$ and tensile meridian for $\sigma_{hor} < \sigma_{ver}$. The example of loading paths in the octahedral stress space with failure points on failure surface were presented in Figure 1.

The shape of the failure surface for elastic-plastic material model in plane of main meridians is described by straight line (in high hydrostatic compression stress region) and tangentially coupled by part of parabola (in small hydrostatic compression and tension stress regions). The trace of failure surface in deviatoric cross-section is determined according to three parametrical *Willam-Warnke* criterion [10] – the hexahedron from criterion of *Coulomb-Mohr* is circumscribed by three ellipses which are tangentially coupled.

3. DESCRIPTION OF FAILURE SURFACE FOR MORTAR AND BRICK

The failure surfaces for the brick and mortar were determined individually. The results of two various series of laboratory experiments were adopted. Methods of preparing the specimens were identical. Mortar specimens were prepared in special moulds, while brick specimens were cut out of the wall specimen.

The data presented here refers to two sets of the specimens. The first set was composed of 23 specimens (symbol M) and the second set contains 16 mortar specimens presented in [9] (symbol Z). Both sets of specimens (M and Z) were prepared according to the same recipe – 1:1:6 (cement : lime : sand). Results of experiments were published partially also in [11], [12]. To establish uniaxial compression strength f_c , modulus of elasticity E_0 and Poisson coefficient ν_0 some of these tests were carried out in uniaxial state of stress. The mean values of these material parameters for mortar are presented in Table 1.

Although compositions of ingredients for mortar Z

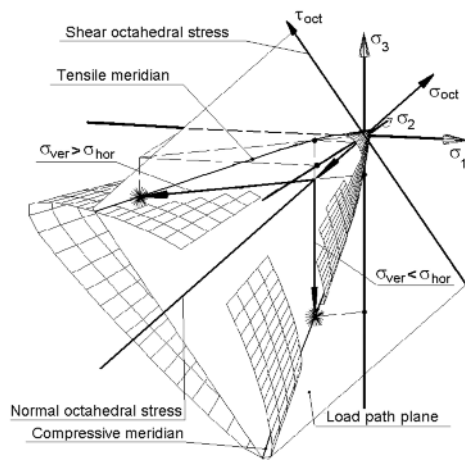


Figure 1. Loading paths in space of stress and 3D shape of failure surface

Table 1. Material parameters for mortar in uniaxial compression tests

Property		Mortar Z	Mortar M	Mean value	
Uniaxial compressive strength	f_{cm}	MPa	-7.39	-8.03	-7.71
Modulus of elasticity – initial value	E_{0m}	MPa	7530	9956	8743.7
Poisson ratio – initial value	ν_{0m}	-	0.161	0.172	0.1669
Vertical strain at failure ($\sigma_{ver,max}$)	ϵ_{cm}	%	-4.14	-1.60	-2.87

and M were identical the stresses at the failure were different. Nevertheless, it did not have a significant influence on the shape of failure surface and its position in the space of octahedral stresses.

The triaxial compression tests were carried out in two steps. In first phase of loading, hydrostatic compression ($\sigma_{ver} = \sigma_{hor}$) was applied. In second phase one of these stresses remained constant, while the second one was increased until the specimen failure. In the case when failure was caused by vertical stress (σ_{ver}) and horizontal stress had constant value, the failure points in space of stress were located along main compressive meridian. In the case of constant vertical stress (σ_{ver}), when the specimens failure was reached by the increased horizontal stress σ_{hor} , the points of failure were concentrated along main tensile meridian. Uniaxial compression tests ($\sigma_{hor}=0$) were also considered in analyses, as a particular case of stress state. The results of laboratory tests for both sets of mortar specimens (set Z and M) were widely presented in [13]. The location of failure points in space of octahedral stresses was shown in Figure 2. This figure presents trace of failure points in main meridian cross-section. The shape of failure surface (cross-section in main meridian plane) was described by main meridian which consists of straight line and tangentially connected parabolic curves. One common description for different types of mortar was achieved thanks to expressing results of laboratory tests with the use of octahedral stress equivalents (normal and shear). The appropriate stress equivalents are represented by the dimensionless values, obtained by dividing the respective stresses (σ_{oct} , τ_{oct}) by the uniaxial compressive strength (f_c).

Experiments for brick and mortar were conducted in

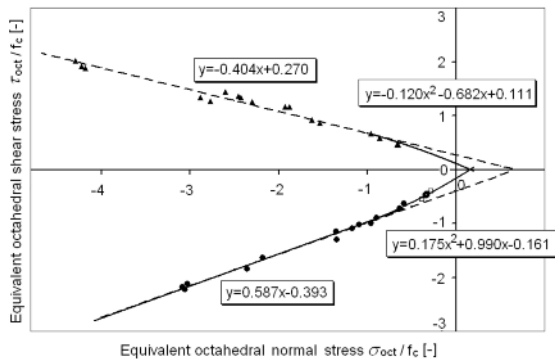


Figure 2. Main meridians for mortar and failure points from laboratory experiments

a similar way. Two sets of brick specimens (16 specimens in first set and 15 in second one) were tested in laboratory [13]. Old and new tests were signed with symbols C and B respectively. Basic material parameters obtained in uniaxial tests were presented in Table 2.

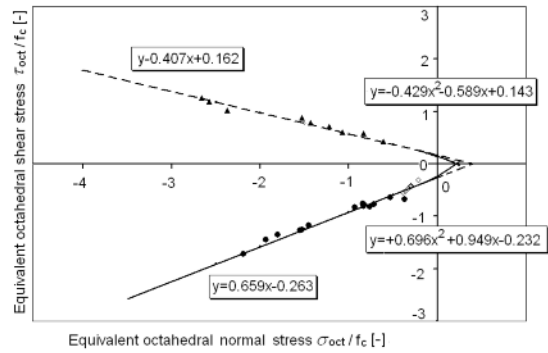


Figure 3. Main meridians for brick and failure points from laboratory experiments

Results of individual tests for brick and their approximation represented by the traces of tension and compression main meridians were shown in Figure 3. As for mortar, the same coordinate system composed of equivalent normal (σ_{oct}/f_c) and shear (τ_{oct}/f_c) octahedral stresses was used.

Divergence between experimental results τ_{oct}/f_c and theoretical approximation of failure surface (main meridians for brick and mortar) was not so significant. Coefficients of determination (R2) fluctuate within the range from 0.916 (for brick) to 0.989 (for mortar). Lower R2 value for brick was a consequence of significant error that appeared for one specimen with probably hidden microcracks.

Main meridians of failure surface for mortar and brick can be described with the use of dependencies:

$$\frac{\tau_{oct}}{f_c} = a \cdot \left(\frac{\sigma_{oct}}{f_c}\right)^2 + b \cdot \frac{\sigma_{oct}}{f_c} + c \quad \text{for } \frac{\sigma_{oct}}{f_c} \geq s_m \quad (7)$$

$$\frac{\tau_{oct}}{f_c} = \alpha \cdot \frac{\sigma_{oct}}{f_c} + \beta \quad \text{for } \frac{\sigma_{oct}}{f_c} \leq s_m \quad (8)$$

The coefficients of equations (7) and (8) were listed in Table 3. Coefficients a , b , c in (7) and α , β in (8) respectively define location of parabolic and linear parts of failure surface main meridians.

Table 2.
Material parameters for bricks in uniaxial compression tests

Property			Brick C	Brick B	Mean value
Uniaxial compressive strength	f_{cb}	MPa	-11.50	-10.21	-10.85
Modulus of elasticity – initial value	E_{0b}	MPa	1931	1947	1937.7
Poisson ratio – initial value	ν_{0b}	-	0.224	0.226	0.2251
Vertical strain at failure ($\sigma_{ver,max}$)	ϵ_{cb}	%	-5.76	-3.61	-4.69

Table 3.
Coefficients for equations describing main meridians of failure surfaces for mortar and brick

Material	Main meridian of	Coefficient					Tangential point
		a	b	c	α	β	$s_m = \sigma_{oct}/f_c$
Mortar	compression	-0.175	-0.990	0.161	-0.587	0.393	-1.1511
	tension	-0.120	-0.682	0.111	-0.404	0.270	
Brick	compression	-0.696	-0.949	0.232	-0.659	0.263	-0.2085
	tension	-0.429	-0.586	0.143	-0.407	0.162	

4. MASONRY SAMPLES USED IN EXPERIMENTS AND NUMERICAL ANALYSIS

In the second stage of investigation, standard masonry samples were tested experimentally. For this purpose, masonry specimens prepared according to standard [8] were used. Results of these tests were widely described in [14]. Masonry specimens (rectangular prisms with external dimensions: 510 x 665 x 120 mm) were composed of 9 brick layers. Experiments were supplemented with computational simulation with the use of the computational system called MAFEM3D developed by *Majewski* and described in [1]. Because of the sample and load symmetry about three perpendicular planes, numerical analysis of the model representing 1/8 of total specimen was carried out. To achieve appropriate imitation of the real masonry sample behaviour, displacements for nodes laying on the planes of symmetry in directions perpendicular to these planes were constrained. Model of the masonry tested in laboratory, as well as its representation used in numerical calculation was shown in the Figure 4.

In numerical simulations, mechanical properties of brick and mortar were modelled independently. Whole specimen have been represented by the finite element mesh, where size of elements was matched to the size of bricks and joints. Each FEM element

was built of exactly one material type. Numerical models created in such a manner were composed of 1944 elements (rectangular prisms) and 2660 nodal points. Length of the elements sides varied within the range between 5.0 and 16.25 mm. Loading of the sample was accomplished by the forced displacements of FEM nodes lying at the top plane of the model. It represented, movement of the testing machine head. In numerical calculations, total displacement assumed amounted to 2 mm. This forced displacement were divided into 40 equal steps. It gave the displacement 0.05 mm per each step. Because of some differences (between two series of experiments) in mechanical properties of analysed materials, mean values were assumed (Table 1 for mortar and Table 2 for brick). In FEM computer system

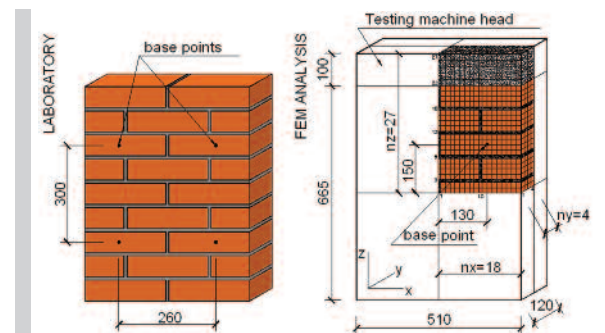


Figure 4.
Experimental and numerical models of masonry specimens

MAFEM3D, these mechanical properties were implemented in the form of mathematical description. The initial values of mechanical parameters shown in Tables 1 and 2 were used directly in numerical calculations. Variability of these parameters was described by the relations used in MAFEM3D system, depending on the effort level (position in space of octahedral stresses).

During laboratory tests four base points were fixed on the front and back side of the real specimen. These stabilised points were utilized for measuring displacements and enabled determination of the strains. Continuous survey of mutual displacements of the base points delivered data for further analysis. Comparison of the experimental and numerical models behaviour was based on displacements values read for these selected points. In numerical calculations displacements have been determined after each step of incrementally realised loading. Comparison of relations between stresses and strains determined in laboratory tests and in numerical calculations is presented in the Figure 5. Points and diagrams on the left side from the ordinate axis represent changes of vertical strains, while points on the right side represent strains in horizontal direction.

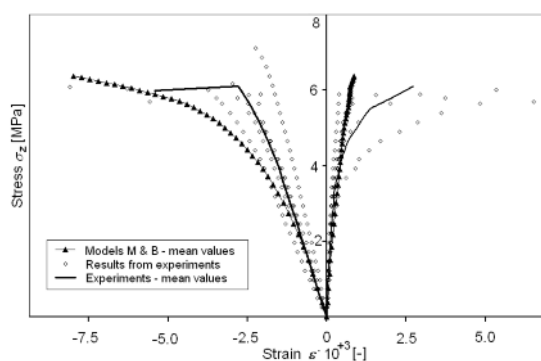


Figure 5.
 σ - ε relations obtained in experimental tests and numerical analysis of heterogeneous masonry samples

Second value compared was mean vertical stress σ_z determined in the horizontal plane of symmetry. It was observed in experimental tests, that beginning of structure damage in the form of visible cracks occurred at the moment, when mean normal, vertical stress achieved value $\sigma_{cr,lab} = -2.88$ MPa. On the other hand, in numerical simulations first symptoms of defects (when stress path reached failure surface for some FEM elements) were observed in 7th step of loading (effort level for the 6th step of loading repre-

sents moment just before cracking). This loading stage corresponded to mean compressive stress in vertical direction equal to $\sigma_{y,num,7} = -2,18$ MPa. In damaged elements, failure surface was reached for relatively high hydrostatic compressive stress level. For relatively low hydrostatic stress failure surface was reached by stress path in 13th step of loading (which is accompanied by splitting cracks). This loading increment corresponded to mean vertical compressive stress $\sigma_{z,num,13} = -3,72$ MPa. The highest recorded value of vertical stress measured in laboratory tests was equal to $\sigma_{z,max,lab} = -6,15$ MPa. Corresponding highest value of vertical stress achieved in numerical simulation was equal to $\sigma_{z,max,num} = -6,37$ MPa. For this load level, number of damaged elements increased rapidly. In the subsequent loading steps, increase of forced displacement at the top surface was followed by the slow decrease of the resultant vertical force (being a sum of vertical stresses σ_z read for one selected horizontal layer of finite elements). Reduction of resultant vertical force was treated as an evidence of exhausting of the load bearing capacity for the masonry specimen. Increase of damaged finite elements for the subsequent load increments is presented in the Figure 6. Loss of load bearing capacity is measured by the factor called effort level, which describe ratio of the current octahedral shear stress to octahedral shear stress corresponding to failure surface (determined for the same normal octahedral stress level). In finite elements marked with a black colour, stress path reached failure surface.

5. NUMERICAL ANALYSIS OF THE HOMOGENEOUS MASONRY STRUCTURE

In the consecutive step of the analysis, the definition of the homogeneous material model for the masonry specimen representation was made. It was the attempt of material model creation for the masonry, which could substitute heterogeneous material description. Such a homogeneous representation of the masonry turned out to be suitable and essential in case of numerical simulation of natural-scale structures. In such calculations, singular finite element must represent comparatively large part of the masonry structure, where several bricks and joint layers must be included. Parameters of the homogeneous model were determined by the comparison of results obtained from numerical simulations with the use of heterogeneous and homogeneous material definitions. Geometrical models (number and

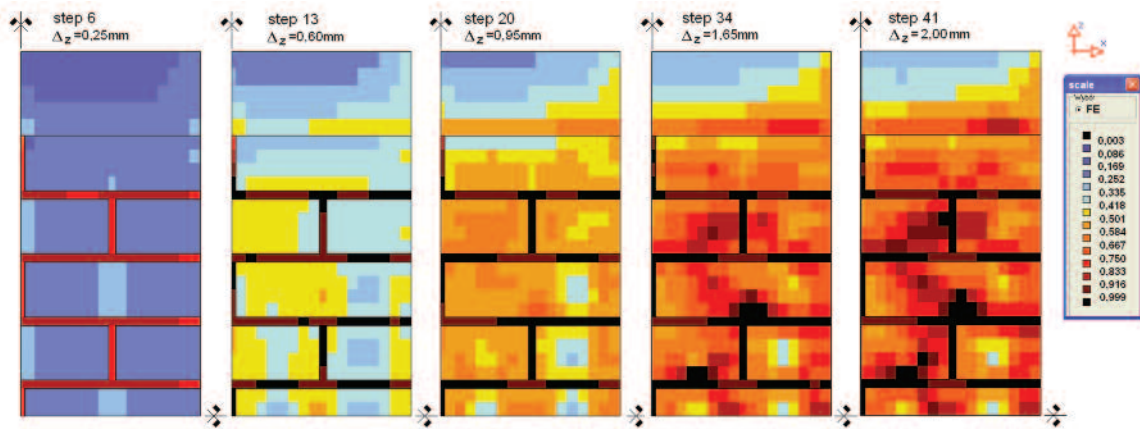


Figure 6. Effort level in FEM model in heterogeneous masonry sample for chosen load increment

arrangement of finite elements) used for the analyses were identical in both cases (Figure 4). Homogeneous masonry model adopted for the numerical calculations was based on the failure surface equations for the brick. Dimensionless (obtained by division of the octahedral stress by the uniaxial compressive strength f_c) equations of the failure surface for the brick were sustained (Figure. 3). Final position of the failure surface for the homogeneous material was derived, considering new (modified) uniaxial compressive strength of the masonry sample treated as a whole. Compressive strength value was adopted from the experimental tests [14] made in uniaxial conditions. For the analysed masonry this strength amounted to $f_c = -6.15$ MPa. The remaining initial parameters (E_0 , ν_0 and ϵ_c) needed for mathematical description of the homogeneous model were assumed proportionally to the relation between uniaxial compressive strength for the masonry and brick. Equations describing main meridians in general form are presented in (7) and (8). Appropriate coefficients (needed for mentioned equations) for brick and mortar are shown in Table 3. Values accepted as a para-

eters of the homogeneous masonry model are listed in Table 4.

To achieve higher accuracy of calculations in numerical calculations with the use of homogeneous model total displacement was reduced to 1.2 mm. Whole process of loading was divided into 39 identical incremental steps, so forced displacement in each step amounted to 0.031 mm.

Proposed method led to quite good convergence for vertical strains in both numerical models. Little bit worse similarity was achieved for strains determined in horizontal direction. Comparison of stress-strain relations for numerical calculation with the use of homogeneous model and laboratory experiments have been presented in the Figure 7. Conformabilities of these deformations confirmed satisfactory assumption of the failure surface for the homogeneous model.

The highest vertical normal stress in numerical analysis with the use of homogeneous model (Hom) was obtained in 36th load increment. Its value amounted to $\sigma_{z,max} = -6.55$ MPa. In the same loading phase,

Table 4. Basic material properties assumed in homogeneous model

Property			Value
Uniaxial compressive strength	f_c	MPa	-6.15
Modulus of elasticity – initial value	E_0	MPa	2874
Poisson ratio – initial value	ν_0	-	0.224
Vertical strain at failure ($\sigma_{ver,max}$)	ϵ_c	%	-2.60

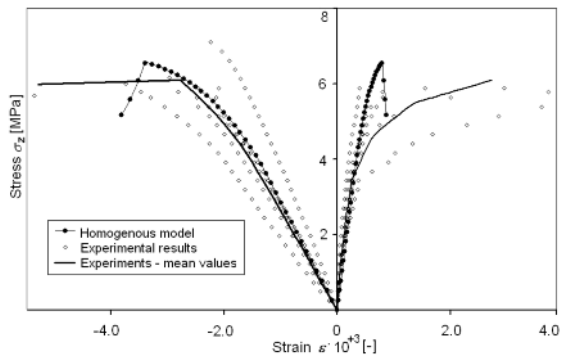


Figure 7.
 σ - ε relations obtained in experimental tests and numerical analysis (homogeneous material model) of masonry samples

forced displacement at the top of the numerical sample (at the plane of contact between head of testing machine and sample) was equal 1.08 mm. Development of the effort level for the finite elements structure for various steps of loading is presented in the Figure 8. Starting from 37th step, when vertical stress σ_z started getting smaller, first damaged (black coloured) elements could be observed. Damaged finite elements area develop rapidly, which could be clearly observed in the Figure 8 (for the 39th load increment). Forced displacement at the top of the sample for this stage of loading achieved value amounted to 1,17mm and corresponding mean vertical stress decreased to $\sigma_{z39} = -5.17$ MPa.

It could be stated that deformation mode and highest stress level achieved in numerical analyses are similar to the corresponding results reached in laboratory experiments.

6. SUMMARY AND CONCLUSIONS

The experiments conducted in triaxial compression apparatus enabled to describe a location of main meridian in octahedral space of stresses. The main meridians (compressive and tensile) look to be sufficient for description of failure surface. Accepted shapes of main meridians consists of straight lines for mean and high normal compression stress and tangentially coupled parabolic curves in small compression and tension stress prove fairly good agreement with experimental data. Differences between experimental data and theoretical description of main meridians are relatively small (except for a few tests). It proves the good choice of failure surface shape.

Description of functions defining location of the failure surfaces for brick and mortar determined a basis for numerical analyses of wall structures. Such a determination of failure surface allows to apply elastic-plastic criteria for multiaxial state of stress.

Complete numerical simulation of the masonry structure is difficult to carry out. Masonry, being a composite of two different materials is not easy to analyse. Appropriate mathematical description of the mechanical properties of masonry and its sufficient precision is difficult to achieve. Solution became more difficult because of masonry structure, which is composed of small pieces (bricks and joints). In physically nonlinear analysis of large-scale masonry structures, it is not possible to use separate models for each composite material due to small size of singular pieces. In this paper, the use of homogeneous (common for brick and mortar) elastic-plastic material model for the numerical analysis was described. The whole analysis was done in several stages. Failure sur-

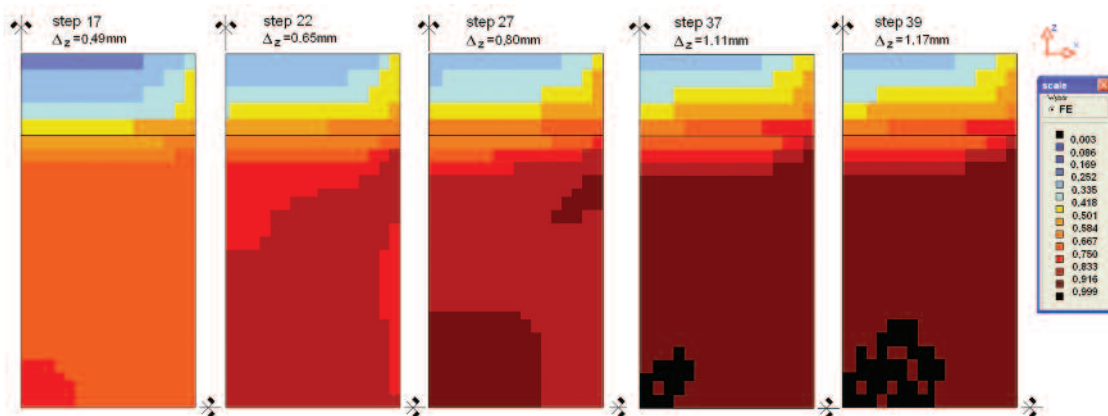


Figure 8.
Effort level in elements of FEM structure of the masonry sample modelled with the use of homogeneous material model obtained for successive load increments

faces for brick and mortar were defined in laboratory tests with the use of triaxial cell. In next steps numerical models of masonry specimens modelled with the use of heterogeneous and homogeneous were created. Material properties in heterogeneous models were directly derived from triaxial tests, while homogeneous masonry model was based on the model for brick. Homogeneous model for the masonry was based on approximated, dimensionless failure surface for brick. Transformation from failure surface for brick to failure surface for masonry was done by scaling, where scale factor was assumed as equal to ratio of uniaxial strength for masonry and brick. In the last step, homogeneous material model was verified. This verification was made by means of comparison of both numerical tests.

On each stage of this analysis, stress-strain relations were verified with the results of experiments carried out on standard masonry specimens. Quite good convergence of described tests was obtained.

REFERENCES

- [1] *Majewski S.*; *Mechanika betonu konstrukcyjnego w ujęciu sprężysto-plastycznym (Mechanics of structural concrete in terms of elasto-plasticity)*. Gliwice 2003, pp. 186.
- [2] *Drobiec Ł.*; *Analiza murów z cegły pełnej ze zbrojeniem w spoinach wspornych poddanych obciążeniom pionowym (Analysis of brick walls with reinforcement in bed joint under vertical loading)*. Rozprawa doktorska (PhD dissertation), Gliwice 2004, pp. 183.
- [3] *Jasiński R.*; *Nośność i odkształcalność zbrojonych ścian murowych ścinanych poziomo (Load bearing capacity and deformability of reinforced brick walls sheared horizontally)*. Rozprawa doktorska (PhD dissertation), Gliwice 2005, pp. 207.
- [4] *Piekarczyk A.*; *Nośność i odkształcalność zbrojonych ścian murowych poddanych ścinaniu w kierunku pionowym (Load bearing capacity and deformability of reinforced brick walls subjected to vertical shearing)*. Rozprawa doktorska (PhD dissertation), Gliwice 2005, pp. 200.
- [5] *Blackard B., Kim B., Citto C., Willam K., Mettupalayam S.*; *Failure issues of brick Masonry*, in: *Fracture Mechanics of Concrete and Concrete Structure*, vol. 3, *High-Performance Concrete, Brick-Masonry and Environmental Aspects*, eds.: *Carpinteri A. et al.*, Taylor & Francis, London 2007, 1587-1594.
- [6] *Carpinteri A., Invernizzi A., Lacidonga G.*; *Numerical simulation of brick-masonry subjected to the double flat-jack tests*, in: *Fracture Mechanics of Concrete and Concrete Structure*, vol. 3, *High-Performance Concrete, Brick-Masonry and Environmental Aspects*, eds.: *Carpinteri A. et al.*, Taylor & Francis, London 2007, 1623-1630.
- [7] *Rots J.G., Boonpichetvong M., Belletti B., Invernizzi S.*; *An application of sequentially linear analysis to settlement damage prediction for masonry facades*, in: *Fracture Mechanics of Concrete and Concrete Structure*, vol. 3, *High-Performance Concrete, Brick-Masonry and Environmental Aspects*, eds.: *Carpinteri A. et al.*, Taylor & Francis, London 2007, 1653-1660.
- [8] *PN-EN 1052-1:2000 Metody badań murów. Część 1: Określenie wytrzymałości na ściskanie (Methods of masonry testing. Part 1: Determining compression strength)*.
- [9] *Szojda L.*; *Analiza współdziałania murowanych budynków ścianowych z deformującym się podłożem (Analysis of interaction of brick wall buildings with deforming subsoil)*. Rozprawa doktorska (PhD dissertation), Gliwice 2001, pp. 180.

- [10] *Willam K. J., Warnke E. P.*; Constitutive Models for the Triaxial Behaviour of Concrete. IABSE Seminar on Concrete Structures Subjected to Triaxial Stresses, Bergamo 1974. IABSE Proc. vol. 19, pp. 1-30.
- [11] *Litewka A., Szojda L.*; Damage, plasticity and failure of ceramics and cementitious composites subjected to multi-axial state of stress, *International Journal of Plasticity*, 11, 22 (2006), 2048-2065.
- [12] *Litewka A., Szojda L.*; Fracture criterion for brick and mortar subjected to tri-axial state of stress, in: *Fracture Mechanics of Concrete and Concrete Structure*, vol. 3, High-Performance Concrete, Brick-Masonry and Environmental Aspects, eds.: *Carpinteri A. et al.*, Taylor & Francis, London 2007, 1605-1612
- [13] *Szojda L., Wandzik G.*; Powierzchnie graniczne dla cegły i zaprawy określone w trójosiowym stanie naprężenia (Boundary surfaces for brick and mortar determined in three-axial state of stress). *Problemy Naukowo-Badawcze Budownictwa, tom II, Konstrukcje Budowlane i Inżynierskie (Scientific-Research Problems of Civil Engineering, volume II, Building and Engineering Constructions)*. Wydawnictwo Politechniki Białostockiej (Publishing house of Białystok University of Technology), Białystok 2007, pp. 363-370.
- [14] *Drobiec Ł., Jasiński R., Kubica J.*; Wstępne badania różnych sposobów wzmocnienia zarysowanych murów ściskanych (Preliminary tests on various ways of cracked compressed walls strengthening), Raport końcowy BK-259/RB-2/97 (Final report), Politechnika Śląska, Wydział Budownictwa, Katedra Konstrukcji Budowlanych, Gliwice, styczeń 2000 r.